Observation of Breathing Dark Pulses in Normal Dispersion Optical Microresonators

Chengying Bao,[1,*] Yi Xuan,[1,2] Cong Wang,[1] Attila Fülöp,[3] Daniel E. Leaird,[1] Victor Torres-Company,[3] Minghao Qi,[1,2] and Andrew M. Weiner[1,2,†]

[1]*School of Electrical and Computer Engineering, Purdue University, 465 Northwestern Avenue, West Lafayette, Indiana 47907-2035, USA*

[2]*Birck Nanotechnology Center, Purdue University, 1205 West State Street, West Lafayette, Indiana 47907, USA*

[3]*Photonics Laboratory, Department of Microtechnology and Nanoscience, Chalmers University of Technology, SE-412 96 Gothenburg, Sweden*

(Received 8 June 2018; published 21 December 2018)

Breathers are localized waves in nonlinear systems that undergo a periodic variation in time or space. The concept of breathers is useful for describing many nonlinear physical systems including granular lattices, Bose-Einstein condensates, hydrodynamics, plasmas, and optics. In optics, breathers can exist in either the anomalous or the normal dispersion regimes, but they have only been characterized in the former, to our knowledge. Here, externally pumped optical microresonators are used to characterize the breathing dynamics of localized waves in the normal dispersion regime. High-Q optical microresonators featuring normal dispersion can yield mode-locked Kerr combs whose time-domain waveform corresponds to circulating dark pulses in the cavity. We show that with relatively high pump power these Kerr combs can enter a breathing regime, in which the time-domain waveform remains a dark pulse but experiences a periodic modulation on a time scale much slower than the microresonator round trip time. The breathing is observed in the optical frequency domain as a significant difference in the phase and amplitude of the modulation experienced by different spectral lines. In the highly pumped regime, a transition to a chaotic breathing state where the waveform remains dark-pulse-like is also observed, for the first time to our knowledge; such a transition is reversible by reducing the pump power.

DOI: 10.1103/PhysRevLett.121.257401

The interaction between nonlinearity and dispersion leads to various localized waves. Breathers are a type of localized wave that occurs in a wide variety of physical systems [1–5]. Unlike solitons which preserve their shape as they propagate, breathers feature periodic variation in time or space. Systems in which breathers exist include Bose-Einstein condensates (BEC) [5], granular lattices [6], micromechanical oscillator arrays [7], nonlinear electrical networks [8], pendula arrays [9], hydrodynamics [2,10], and optics [4,11]. Optical systems are widely used to study breathers due to the ease of tailoring the linear and nonlinear properties of the systems. Optical breathers were first studied in conservative systems, namely optical fibers [4,11]. Recently bright soliton breathers have also been observed in dissipative systems such as externally pumped fiber cavities [12,13] and microresonators [14–17].

In optics, the character of the nonlinear dynamics depends strongly on the sign of the dispersion, i.e., derivative of the reciprocal of group velocity with optical frequency. To date optical breathers have been explored primarily in the anomalous dispersion regime, under which group velocity increases with frequency; the joint action of anomalous dispersion and a self-focusing nonlinearity gives rise to bright solitons. Here, we consider the nonlinear dynamics in the opposite, normal dispersion regime, again with a self-focusing nonlinearity. In principle, equivalent nonlinear dynamics should also occur for one-dimensional spatial diffraction with a defocusing nonlinearity [18]. Dark solitons, which have been reported in optics [18,19], BEC [20], and hydrodynamics [21], exist in this regime. Although breathing dark pulses (also termed dark soliton breathers) have been predicted to exist in normal dispersion microresonators [22,23], experimental study of optical breathing dark pulses has been limited in conservative as well as dissipative optical systems, to our knowledge.

In this Letter, we present the first experimental study focusing on optical breathing dark pulses in the normal dispersion regime using microresonators. Kerr comb generation in normal dispersion microresonators [22–29] provides this unique opportunity. We find that although the dark pulses breathe relatively gently, different spectral lines can exhibit clear differences in the modulation depth and phase with which they breathe. In the highly driven regime, we observe that the breathing dark pulse in our dissipative cavity can reversibly enter a chaotic state, where the waveform remains dark localized and similar to that of the stable or the breathing dark pulse. The breathing dark pulse dynamics in dissipative cavities is governed by the Lugiato-Lefever equation (LLE), i.e., driven-damped nonlinear Schrödinger equation [30–33]. Indeed, our experimental observations are consistent with numerical simulations based on the LLE. Moreover, simulations reveal the importance of modulation of switching waves (also termed as domain walls or fronts) [24,34,35] in the breathing dynamics.

We start our investigation with simulations based on the LLE [12,30,33], which can be written as

$$\left(t_R\frac{\partial}{\partial t}+\frac{\alpha}{2}+i\delta_0+i\frac{\beta_2 L}{2}\frac{\partial^2}{\partial\tau^2}\right)E-i\gamma L|E|^2E=\sqrt{\kappa}E_{\mathrm{in}}, \qquad (1)$$

where E is the envelope of the intracavity field, t and τ are slow time and fast time variables, respectively, t_R and L are the round trip time and cavity length, β_2 and γ are the group velocity dispersion and nonlinearity coefficient, α and κ are the total loss and coupling loss, E_{in} is the amplitude of the pump field, and δ_0 is the pump phase detuning (angular frequency detuning to the closest resonance multiplied by t_R). Simulation parameters used are $t_R = 4.3$ ps, $\beta_2 = 187\ \mathrm{ps}^2/\mathrm{km}$, $L = 628\ \mu\mathrm{m}$, $\gamma = 0.9\,(\mathrm{Wm})^{-1}$, $\alpha = 0.0068$, $\kappa = 0.0054$, which are close to experimental parameters and enable direct comparison with experiments. The simulation starts with a noise field in the microresonator, and the detuning δ_0 is tuned to generate the comb [see the Supplemental Material [36] for a detailed view of the path to comb generation]. A breathing dark pulse is obtained with a pump power of 700 mW (64% of the experimental on-chip power) and a final detuning of 0.0629 radians (equivalent to a laser frequency 2.3 GHz to the red of the resonance). We show the simulated breathing dynamics together with representative spectra and waveforms in Fig. 1. Both the power spectrum and the temporal intensity profile of the comb vary periodically, repeating with a period of 1.3 ns (782 MHz), ~300 times longer than t_R. The formation of dark pulses can be understood as arising from interlocked switching waves, which are traveling front solutions connecting the bistable homogeneous state of the LLE [24,34,35]. The background field (i.e., the high power part of the dark-localized waveform) stays nearly unchanged during the breathing cycle, because it follows the homogeneous stable state [22,23,34]. Because the background field carries most of the comb power (average power over one round trip time), the breathing depth of the comb power, which is defined as $(P_{\max}-P_{\min})/(P_{\max}+P_{\min})$ with $P_{\max(\min)}$ being the maximum (minimum) power, is relatively low. The simulated breathing depth of the intracavity comb power including (excluding) the pump is 3% (6%). During the breathing, the switching waves are modulated as illustrated both by Fig. 1(b) and Animation 1. The corresponding modulation in the tails of the switching waves results in the stronger breathing in the waveform hole (the low power part of the dark-localized waveform). Because the dark pulse has a complex waveform, the breathing within the waveform hole is also complex.

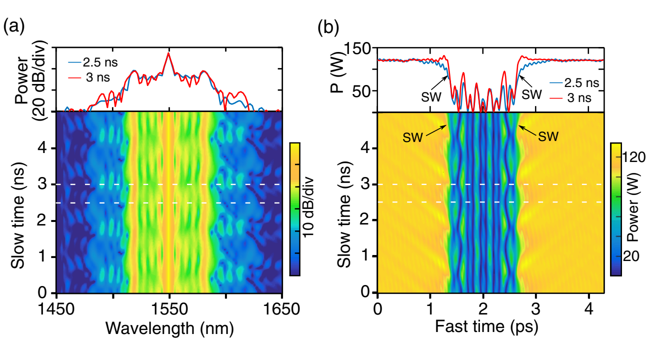

FIG. 1. (a) Simulated breathing dynamics of optical power spectrum, showing complex breathing behavior. (b) Simulated breathing dynamics in the time domain. The switching waves (SWs) are modulated during breathing and the waveform hole breathes strongly. Above each panel we show snapshots of the spectrum and time-domain waveform at moments indicated by the dashed lines.

We have performed experiments in three different (see Table I) optical microresonators which provide data supporting the simulated dynamics. We focus our discussion on results from a silicon nitride microresonator (device 1 in Table I) with a radius of 100 μm, a loaded Q factor of 0.8×10^6, geometry of 2000 nm × 600 nm (waveguide width vs height), a free spectral range (FSR) of 231 GHz, and strong normal group velocity dispersion $\beta_2 = 190\ \mathrm{ps}^2/\mathrm{km}$. The experimental setup is sketched in Fig. 2(a). Similar to bright soliton breathers [12,14–16], the breathing dark pulse state exists in a regime with relatively strong pump power and small detuning [22,23]. Hence, we generate our comb with a relatively large on-chip pump power of 1.1 W (obtained by measuring the off-chip power and adjusted with ~2 dB fiber-to-chip coupling loss). By tuning the continuous wave (cw) pump laser into resonance from the blue to the red, we are able to generate a broadband, single FSR comb [Fig. 2(b)]. In this state the comb power measured by a fast photodetector exhibits narrow radio-frequency (rf) tones as shown in Fig. 2(c). The fundamental frequency of the rf tones is 740 MHz, in close agreement with the simulated breathing frequency and much larger than the resonance linewidth which has half-width-half-maximum (HWHM) of 125 MHz. The other normal dispersion devices listed in Table I also show narrow rf tones that can be attributed to dark pulse breathing, supporting the generality of our observation. The observed breathing frequencies decrease with increasing loaded Q factor (decreasing resonance linewidth).

TABLE I. Measured breathing frequencies, loaded Q factor, and HWHM resonance linewidths for three microresonators with similar 231 GHz FSRs.

	Frequency	Loaded Q	Resonance HWHM
Device 1	~740 MHz	$\sim 0.8\times10^6$	~125 MHz
Device 2	~635 MHz	$\sim 1\times10^6$	~100 MHz
Device 3	~250 MHz	$\sim 2.4\times10^6$	~40 MHz

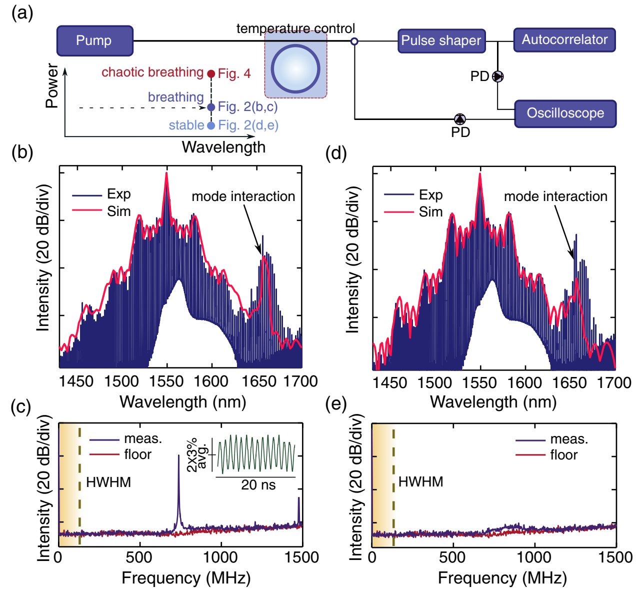

FIG. 2. (a) Experimental setup and summary of comb states. A pulse shaper is used to select individual comb lines; their fast breathing dynamics are recorded individually using a fast photodetector (PD) and digital oscilloscope. When recording the fast breathing dynamics, a portion of the breathing comb is used to trigger the oscilloscope to provide a timing reference. By controlling the pump power, both periodic breathing and chaotic breathing are experimentally studied. The chip is placed on a temperature controlled stage. (b), (c) Optical and rf spectrum of the breathing dark pulse state under an on-chip power of 1.1 W. The simulated optical spectrum is in close agreement with the measured spectrum. The breathing dark pulse state has narrow rf tones on the rf spectrum, whose frequencies are outside the half-width-half-maximum (HWHM) of the resonance. The inset in (c) is the measured comb power change of the breathing dark pulse (including pump line) at the through-port, showing a weak modulation depth of ~3%. (d), (e) Optical and rf spectrum of the stable dark pulse state under an on-chip power of 1.0 W. There is no significant difference in the averaged optical spectra between the breathing and stable state.

In each case, the breathing frequency is approximately six times the HWHM resonance linewidth. Similar narrow rf tones were previously observed in a normal dispersion microresonator, but without experimental evidence to show the comb corresponds to breathing dark pulse [24]. Here, we confirm that the comb in Figs. 2(b) and 2(c) corresponds to a breathing dark pulse and attribute the rf tones to periodic modulation of the comb lines.

The measured optical spectrum of the breathing state is in close agreement with the averaged simulated optical spectrum [see Fig. 2(b)]. Furthermore, the overall modulation of the breathing dark pulse is weak, also in agreement with simulation. The comb power measured at the through port including (excluding) the pump line breathes with a depth of ~3% (~5%). This is significantly different from bright soliton breathers, for which the modulation of the comb power excluding the pump can reach ~50% [14]. We can transition to a stable dark pulse state by reducing the pump power to 1.0 W at the same wavelength and can return to the breathing state by increasing the pump power back to 1.1 W. At the lower pump power, the comb shows low-noise operation [Figs. 2(d) and 2(e)]. Again, the simulated stable dark pulse gives an optical spectrum in agreement with experiment. The time averaged optical spectra of the breathing and stable dark pulse combs show no significant difference. This is a consequence of the weak overall breathing and is a key difference with respect to bright soliton breathers [14,16]. There is a spike in the spectrum around 1657 nm due to interaction with another spatial mode, which is reproduced by inclusion of mode interaction in the simulations [see the Supplemental Material [36]]. Note that the existence of mode interaction was observed to cause intermode breathing in one recent report on anomalous dispersion microresonators [17]. We have verified that mode interaction is not responsible for the observed breathing in our experiments by changing the chip temperature to a value where the mode interaction effects vanish [see the Supplemental Material [36]].

To establish the observation of a breathing dark pulse, we first need to verify that the comb in Figs. 2(b) and 2(c) has a dark-localized waveform. We use line-by-line pulse shaping to probe the corresponding waveform [24,39,40]. By adjusting the phases of the comb lines to compress them into a transform-limited pulse train, we can retrieve the comb phase profile and the corresponding waveform [see the Supplemental Material [36] for methods]. In experiments, we first adjust the pump power to reach the stable dark pulse state and apply pulse shaping to compress the output into transform-limited pulses, whose intensity autocorrelations (ACs) are shown in Fig. 3(a). We then adjust the pump power to transition into the breathing state, while keeping the same phase profile on the pulse shaper. The output is still compressed into a transform-limited pulse. This comparison suggests that the breathing dark pulse has a spectral phase profile very close to that of the stable dark pulse. Because the breathing dark pulse only exhibits a gentle modulation, we deduce that the breathing comb retains a dark-localized waveform [inset of Fig. 3(a)]. The simulated AC of the breathing dark pulse after numerical pulse compression and averaging over slow time [i.e., t in Eq. (1)] is close to the AC of the stable comb (see the Supplemental Material [36] for methods to obtain the numerical AC) [Fig. 3(b)]. In experiments on another microresonator (device 2), we have confirmed that a dark-localized waveform is retained during breathing by using an alternative approach based on an optical sampling oscilloscope [see the Supplemental Material [36]].

Next, we confirm that the form of the comb varies periodically and examine the breathing of individual lines. To do that, we program the pulse shaper to select individual comb lines and then measure their time-dependent power using a photodetector. A sample of the full comb is also detected; its power modulation under breathing is used as a

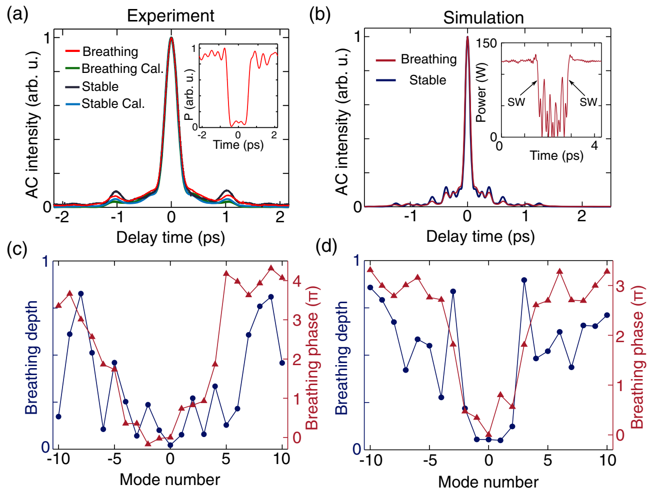

FIG. 3. (a),(b) By line-by-line pulse shaping, stable dark pulses can be compressed into transform-limited pulses (the shaped comb lines contain 90% of the comb power). Applying the same phase on the pulse shaper, the breathing dark pulses can also be compressed into transform-limited pulses. The intensity autocorrelations (ACs) of the compressed pulses are plotted in the figure. Using the phase retrieved in the line-by-line pulse shaping, the actual intracavity field is deduced to have a dark-localized waveform for the breathing Kerr comb (inset). The averaged simulated AC trace of the pulse-shaped breathing dark pulse comb [see the Supplemental Material [36] for numerical methods] is close to the AC of the pulse-shaped stable dark pulse comb. The inset is an example of a snapshot of the breathing dark pulse (SW: switching wave). The AC in simulations is shorter, because it calculates the full spectrum while only a portion of the spectrum is shaped in experiments. (c),(d) The breathing depth (blue) and phase (red) of individual comb lines. The breathing depths tend to be larger at the wings of the spectrum; different lines also breathe with different phases. Both the breathing depth and phase can change abruptly between adjacent lines.

trigger, providing a timing reference to compare the breathing signals and their rf phase delays for different comb lines [Fig. 2(a)]. In experiments, we observe that the absolute breathing amplitudes of the central comb lines within $[-2, 2]$ relative to the pumped mode are much higher compared to other comb lines. However, the average powers are also higher for the central comb lines, and the modulation depths of individual lines tend to be larger in the wings of the spectrum [Fig. 3(c)]. Although the breathing depth of the total comb power is only 3%, some individual lines breathe deeply. Furthermore, the phase of the rf breathing signal varies from line to line [Figs. 3(c) and 3(d)]. Consequently, the comb spectrum is changing during the modulation period, providing definitive proof of a breathing state. The qualitative trend obtained in simulations is similar; see Fig. 3(d). Some of the details of the simulated breathing do differ from the experiments; these may be attributed to the difficulty in modeling the mode interaction accurately and the unconsidered wavelength-dependent Q factor. The phase and amplitude of the breathing can change abruptly from one line to the next; this observation is consistent with the simulated complex breathing dynamics shown in Fig. 1.

The high Q microresonator also enables us to study the breathing dynamics of dark pulses in the highly driven regime. By increasing the on-chip pump power up to 1.3 W, the breathing first exhibits period tripling and then becomes chaotic. The comb in this chaotic state retains the optical spectral features of the dark pulse [Fig. 4(a)], and the averaged spectrum from simulation is in good agreement with the measurement. Animation 2 provides a visualization of the simulated chaotic breathing dynamics. However, the measured rf spectrum shows broadband noise [Fig. 4(b)]; this is also observed in simulations when increasing the pump power to 785 mW under the same detuning as Fig. 1 [Fig. 4(b) inset]. The modulation depth of the chaotic breathing dark pulse is at the few percent level in the simulation, similar to that of the periodic breathing dark pulse. Chaotic breathing was predicted and observed to exist in the LLE with anomalous dispersion [12,13,16,41]; it has also been predicted to exist for breathing dark pulses [22] but not demonstrated until now. Our results constitute the first observation of such a chaotic transition for breathing dark solitary waves in all physical systems, to our knowledge. It is also worth noting that by reducing the pump power at a constant pump frequency, one can move repeatably from the chaotic breathing state back to the periodic breathing or stable state. Note that this chaotic breathing state is distinct from the chaotic state that occurs while tuning the pump frequency prior to reaching the breathing or mode-locked dark pulse state [24]. When we apply the same phase profile used in Fig. 3(a) on the pulse shaper, the AC trace obtained under the chaotic breathing state still shows a clean peak pulse which is close to the transform limit (as calculated from the time averaged spectrum). The visibility of the AC trace exceeds 97%. This observation differs dramatically from reports that unstable modulation instability Kerr combs with broadband noisy rf spectra cannot be compressed into transform-limited pulses [40]. The ability here to compress using the same phase profile as for the stable dark pulse suggests that the comb retains a dark-localized waveform even under chaotic breathing. Consistent with the experimental measurement, the averaged AC trace (in simulation, after numerical pulse shaping) of the chaotic breathing state remains close to the AC of the stable state [Fig. 4(d)].

In summary, optical breathing dark pulses are clearly observed and comprehensively modeled for the first time, using normal dispersion microresonators. The breathing dark pulse features a high frequency modulation and a weak modulation depth. Different comb lines breathe in distinct manners, a behavior which is related to a modulation of the switching waves and their oscillating tails. This behavior is in sharp contrast to the dynamics observed in breathing bright solitons in anomalous dispersion microresonators. At higher pump power, the breathing dark pulse undergoes a

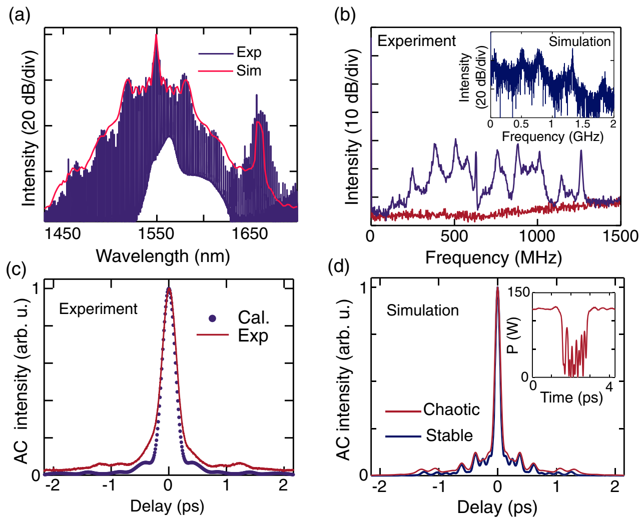

FIG. 4. (a) The averaged experimental and simulated optical spectrum in a chaotic breathing state. (b) Measured broadband rf spectrum in the chaotic breathing state (red line is the noise floor); the inset shows the simulated broadband rf spectrum. (c) The AC of the Kerr comb in the chaotic breathing state after pulse shaping [the same amplitude and phase adjustment used in Fig. 3(a)] is close to the calculated autocorrelation trace of the transform limited pulse. (d) The simulated comb in the chaotic state can also be shaped into transform limited pulse; the inset shows an example of the dark-localized waveform. The compressed pulse in simulations is shorter because it calculates the full spectrum [similar to Figs. 3(a) and 3(b)].

reversible chaotic transition, where a dark-localized waveform is retained despite the broadband intensity noise. The breathing instability can impair applications which need stable combs; knowledge of breathing dark pulses can help us avoid this instability. Our Letter also suggests high Q microresonator can be a useful platform to study nonlinear dynamics, especially in the highly driven regime.

This Letter was supported in part by the Air Force Office of Scientific Research (Grant No. FA9550-15-1-0211), by the DARPA PULSE program (Grant No. W31P4Q-13-1-0018) from AMRDEC, and by the National Science Foundation (Grant No. ECCS-1509578). A. F. and V. T. C. acknowledge partial support by the Swedish Research Council and the European Research Council (DarkComb Grant Agreement No. 771410). C. B. acknowledge partial support from a postdoctoral fellowship from the Resnick Institute, Caltech. We gratefully acknowledge fruitful discussions with Xiaoxiao Xue, Nail Akhmediev, Zhen Qi, and Curtis Menyuk.

*cbao@caltech.edu
Present address: T. J. Watson Laboratory of Applied Physics, California Institute of Technology, Pasadena 91125, USA.
†amw@purdue.edu

[1] E. Kuznetsov, A. Rubenchik, and V. E. Zakharov, Phys. Rep. **142**, 103 (1986).
[2] Y.-C. Ma, Stud. Appl. Math. **60**, 43 (1979).
[3] N. Akhmediev and V. Korneev, Theor. Math. Phys. **69**, 1089 (1986).
[4] B. Kibler, J. Fatome, C. Finot, G. Millot, F. Dias, G. Genty, N. Akhmediev, and J. M. Dudley, Nat. Phys. **6**, 790 (2010).
[5] A. Trombettoni and A. Smerzi, Phys. Rev. Lett. **86**, 2353 (2001).
[6] S. Flach and A. V. Gorbach, Phys. Rep. **467**, 1 (2008).
[7] M. Sato, B. Hubbard, and A. Sievers, Rev. Mod. Phys. **78**, 137 (2006).
[8] L. Q. English, F. Palmero, P. Candiani, J. Cuevas, R. Carretero-González, P. G. Kevrekidis, and A. J. Sievers, Phys. Rev. Lett. **108**, 084101 (2012).
[9] J. Cuevas, L. Q. English, P. G. Kevrekidis, and M. Anderson, Phys. Rev. Lett. **102**, 224101 (2009).
[10] A. Chabchoub, N. P. Hoffmann, and N. Akhmediev, Phys. Rev. Lett. **106**, 204502 (2011).
[11] J. M. Dudley, F. Dias, M. Erkintalo, and G. Genty, Nat. Photonics **8**, 755 (2014).
[12] F. Leo, L. Gelens, P. Emplit, M. Haelterman, and S. Coen, Opt. Express **21**, 9180 (2013).
[13] M. Anderson, F. Leo, S. Coen, M. Erkintalo, and S. G. Murdoch, Optica **3**, 1071 (2016).
[14] C. Bao, J. A. Jaramillo-Villegas, Y. Xuan, D. E. Leaird, M. Qi, and A. M. Weiner, Phys. Rev. Lett. **117**, 163901 (2016).
[15] M. Yu, J. K. Jang, Y. Okawachi, A. G. Griffith, K. Luke, S. A. Miller, X. Ji, M. Lipson, and A. L. Gaeta, Nat. Commun. **8**, 14569 (2017).
[16] E. Lucas, M. Karpov, H. Guo, M. Gorodetsky, and T. Kippenberg, Nat. Commun. **8**, 736 (2017).
[17] H. Guo, E. Lucas, M. H. P. Pfeiffer, M. Karpov, M. Anderson, J. Liu, M. Geiselmann, J. D. Jost, and T. J. Kippenberg, Phys. Rev. X **7**, 041055 (2017).
[18] G. Allan, S. Skinner, D. Andersen, and A. L. Smirl, Opt. Lett. **16**, 156 (1991).
[19] A. M. Weiner, J. P. Heritage, R. J. Hawkins, R. N. Thurston, E. M. Kirschner, D. E. Leaird, and W. J. Tomlinson, Phys. Rev. Lett. **61**, 2445 (1988).
[20] S. Burger, K. Bongs, S. Dettmer, W. Ertmer, K. Sengstock, A. Sanpera, G. Shlyapnikov, and M. Lewenstein, Phys. Rev. Lett. **83**, 5198 (1999).
[21] A. Chabchoub, O. Kimmoun, H. Branger, N. Hoffmann, D. Proment, M. Onorato, and N. Akhmediev, Phys. Rev. Lett. **110**, 124101 (2013).
[22] P. Parra-Rivas, E. Knobloch, D. Gomila, and L. Gelens, Phys. Rev. A **93**, 063839 (2016).
[23] C. Godey, I. V. Balakireva, A. Coillet, and Y. K. Chembo, Phys. Rev. A **89**, 063814 (2014).
[24] X. Xue, Y. Xuan, Y. Liu, P.-H. Wang, S. Chen, J. Wang, D. E. Leaird, M. Qi, and A. M. Weiner, Nat. Photonics **9**, 594 (2015).
[25] Y. Liu, Y. Xuan, X. Xue, P.-H. Wang, S. Chen, A. J. Metcalf, J. Wang, D. E. Leaird, M. Qi, and A. M. Weiner, Optica **1**, 137 (2014).
[26] W. Liang, A. A. Savchenkov, V. S. Ilchenko, D. Eliyahu, D. Seidel, A. B. Matsko, and L. Maleki, Opt. Lett. **39**, 2920 (2014).

[27] V. Lobanov, G. Lihachev, T. Kippenberg, and M. Gorodetsky, Opt. Express **23**, 7713 (2015).

[28] S.-W. Huang, H. Zhou, J. Yang, J. F. McMillan, A. Matsko, M. Yu, D.-L. Kwong, L. Maleki, and C. W. Wong, Phys. Rev. Lett. **114**, 053901 (2015).

[29] J. K. Jang, Y. Okawachi, M. Yu, K. Luke, X. Ji, M. Lipson, and A. L. Gaeta, Opt. Express **24**, 28794 (2016).

[30] L. A. Lugiato and R. Lefever, Phys. Rev. Lett. **58**, 2209 (1987).

[31] S. Coen, H. G. Randle, T. Sylvestre, and M. Erkintalo, Opt. Lett. **38**, 37 (2013).

[32] I. Barashenkov and E. Zemlyanaya, J. Phys. A **44**, 465211 (2011).

[33] Y. K. Chembo and C. R. Menyuk, Phys. Rev. A **87**, 053852 (2013).

[34] P. Parra-Rivas, D. Gomila, E. Knobloch, S. Coen, and L. Gelens, Opt. Lett. **41**, 2402 (2016).

[35] B. Garbin, Y. Wang, S. G. Murdoch, G.-L. Oppo, S. Coen, and M. Erkintalo, Eur. Phys. J. D **71**, 240 (2017).

[36] See Supplemental Material at http://link.aps.org/supplemental/10.1103/PhysRevLett.121.257401, which includes Refs. [37,38], for further experimental and numerical methods; it also includes experimental evidence of the breathing in the time domain.

[37] P.-H. Wang, Y. Xuan, L. Fan, L. T. Varghese, J. Wang, Y. Liu, X. Xue, D. E. Leaird, M. Qi, and A. M. Weiner, Opt. Express **21**, 22441 (2013).

[38] P. A. Andrekson and M. Westlund, Laser Photonics Rev. **1**, 231 (2007).

[39] S. T. Cundiff and A. M. Weiner, Nat. Photonics **4**, 760 (2010).

[40] F. Ferdous, H. Miao, D. E. Leaird, K. Srinivasan, J. Wang, L. Chen, L. T. Varghese, and A. M. Weiner, Nat. Photonics **5**, 770 (2011).

[41] K. Nozaki and N. Bekki, J. Phys. Soc. Jpn. **54**, 2363 (1985).